

Zenith-Distance Dependence of Chromatic Shear Effect: A Limiting Factor for an Extreme Adaptive Optics System

Tadashi Nakajima

*National Astronomical Observatory of Japan
Osawa 2-21-1, Mitaka, 181-8588, Japan*

ABSTRACT

Consider a perfect AO system with a very fine wavefront sampling interval and a very small actuator interval. If this AO system senses wavefront at a wavelength, λ_{WFS} , and does science imaging at another wavelength, λ_{SCI} , the light paths through the turbulent atmosphere at these two wavelengths are slightly different for a finite zenith distance, z . The error in wavefront reconstruction of the science channel associated with this non-common path effect, or so-called chromatic shear, is uncorrectable and sets an upper bound of the system performance. We evaluate the wavefront variance, $\sigma^2(\lambda_{WFS}, \lambda_{SCI}, z)$ for a typical seeing condition at Mauna Kea and find that this effect is not negligible at a large z . If we require that the Strehl ratio be greater than 99 or 95%, z must be less than about 50 or 60° respectively, for the combination of visible wavefront sensing and infrared science imaging.

Subject headings: atmospheric effects, instrumentation: adaptive optics, instrumentation: high angular resolution

1. Introduction

It is well known that a high-performance adaptive optics system with a Strehl ratio well over 90% is required for the direct detection of an exoplanet from the ground especially in reflected light. Such an adaptive optics system is often called an extreme AO system (ExAO), because of its high level of sophistication in instrumentation. The ExAO has strict requirements on guide stars and wavefront sensors. Fine wavefront sampling is achieved by many pixels in the wavefront sensor, each of which corresponds to the length scale less than cm. Fine temporal sampling is also required along with the fine spatial sampling. Therefore, a large number of photons are required for a tiny area on the wavefront for a short period of time. So an AO guide star must be very bright. Another requirement on the guide star is that it must be regarded as a point source, even after the AO correction, and a presently available laser guide star, located at a finite altitude with a finite angular extent, is not fitted for this purpose, even if the problem of brightness or laser power is

overcome. If the Strehl reduction due to the finite extent of the laser guide star is inevitable, there is no point of sampling the wavefront so finely, in other words, there is no use of an ExAO. For the same reason, a stringent requirement on isoplanicity will result in a small field of view. For these reasons, the major application of an ExAO requires a very bright natural guide star and the high Strehl ratio is achieved only for a small field of view. All things considered, an exoplanet search around bright nearby stars, will remain the primary scientific goal for an ExAO project.

There are many sources of errors that can cause the reduction of the Strehl ratio, e.g. see (Guyon 2005), but most of them are in principle controllable by sophisticated instrumentation. However, there are also some errors which are in principle uncorrectable. Here we focus on one of the major uncorrectable errors: atmospheric chromatic non-common-path error, or “chromatic shear (CS)”, associated with the different paths through the turbulent atmosphere of the light beams incident on the visible wavefront sensor and the infrared science imager, when the target star is at a finite zenith distance.

In actual astronomical observations, total observing time for an object is finite and the object never stays at the zenith. Moreover, it often happens that an object needs to be observed at a large zenith distance, due a large difference between the declination of the object and the latitude of the observatory. In order to secure a significant amount of observing time for an exoplanet search, it is inevitable to observe a target star with a finite zenith distance.

Most of the current AO systems sense wavefront at visible wavelengths and image the target at near-infrared wavelengths. This is partly due to the higher availability of a visible detector such as a CCD for a wavefront sensing camera. However, if the CS effect is a significant limiting factor for the next-generation extreme AO systems whose scientific justification is direct exoplanet detection, the choice of the combination of λ_{WFS} and λ_{SCI} , may need to be reconsidered.

In this paper, we quantify the magnitude of this CS effect, in terms of wavefront variance associated with it.

2. Formulation

2.1. Refractive Index and Atmospheric Model

According to Cox (1999), using the index of refraction, $n_s(\lambda)$, for dry air at a standard pressure, p_s , a standard absolute temperature, T_s , the refractive index n for the pressure, p , and absolute temperature, T , is given by,

$$n(\lambda; p, t) - 1 = \left(\frac{p}{p_s}\right) \left(\frac{T_s}{T}\right) (n_s(\lambda) - 1). \quad (1)$$

Strictly speaking, n is also dependent on the water vapor pressure. However its effect is

a minor reduction of n and the dry air case represents the worst case designing. To obtain the light path through the atmosphere, we need to know the vertical profiles of $p(h)$ and $T(h)$, where h is altitude. We adopt an atmosphere model of the Earth used in the field of aeronautics, in which the pressure and temperature are given as analytic functions of the altitude, h (<http://www.grc.nasa.gov/WWW/K-12/airplane/atmosmet.html>). This model covers from the troposphere ($h > 0$ km) to the stratosphere ($h < 50$ km), while turbulent layers of significance for optical wave propagation is located at altitudes below the lower stratosphere ($h < 25$ km). Then the refractive index n becomes a function of λ , and h .

If the zenith distance of a star incident on the upper atmosphere from space is z_0 , the apparent zenith distance, $z(\lambda, h)$, is related to z_0 by

$$n(\lambda, h) \cdot \sin z(\lambda, h) = \sin z_0. \quad (2)$$

At an arbitrary altitude in the atmosphere, h , Snell's law can be expressed in a differential form as,

$$dn(\lambda, h) \cdot \sin z(\lambda, h) + n(\lambda, h) \cdot \cos z(\lambda, h) \cdot dz = 0. \quad (3)$$

or

$$dz(\lambda, h) = -\tan z(\lambda, h) \cdot dn(\lambda, h)/n(\lambda, h). \quad (4)$$

In principle, we must integrate this differential relation (4) along the light path. However, for the practical purpose, a more useful approximate expression for the bending angle, $\Delta\theta(\lambda, h)$, not in a differential form, is obtained, since the index of refraction of the air is very close to that of the vacuum and the total bending angle is also small. By taking the first order terms of eq(2),

$$\Delta\theta(\lambda, h) = -\tan z_0 \cdot (n(\lambda, h) - 1). \quad (5)$$

To evaluate CS, we need to know the separation of the two beams at λ_{WFS} and λ_{SCI} , perpendicular to the line of sight in length, r , at a given altitude, h and zenith distance, z_0 .

In actual observing with an AO system, an atmospheric dispersion corrector will be used and the two beams are aligned inside the optical system. The two beams gradually separate towards the upper atmosphere and eventually become parallel above the stratosphere.

Since the angle between the two beams, α is given by

$$\alpha(\lambda_{WFS}, \lambda_{SCI}, h) = \Delta\theta(\lambda_{WFS}, h) - \Delta\theta(\lambda_{SCI}, h)$$

$$= -\tan z_0 \cdot (n(\lambda_{WFS}, h) - n(\lambda_{SCI}, h)). \quad (6)$$

We calculate r as follows. Let H_T and H_{MAX} be the altitude of the telescope and the upper limit of the atmosphere. Then a relative ray displacement due to differential refraction, r is obtained by the following integration,

$$r(\lambda_{WFS}, \lambda_{SCI}, h) = \int_{H_T}^h \alpha(\lambda_{WFS}, \lambda_{SCI}, h) / \cos z_0 dh. \quad (7)$$

2.2. Turbulence Model and Wavefront Variance

The turbulence profile is characterized by the refractive index structure constant, $C_n^2(h)$, whose integral is related to the Fried parameter, r_0 (Fried 1966), by

$$r_0 = 0.185 \left[\frac{\lambda_{SCI}^2}{\int_{H_T}^{H_{MAX}} C_n^2(h) dh} \right]^{3/5}. \quad (8)$$

In our calculation, a seeing condition is specified by r_0 at a given wavelength, λ_{SCI} . Then from eq(8), the integral of C_n^2 , $\int_{H_T}^{H_{MAX}} C_n^2(h) dh$ is obtained. For a good seeing condition typical of an astronomical site, the variation of $C_n^2(h)$ as a function of h is slow. Under such conditions, the wave propagation through a turbulent medium can be treated by “smooth perturbations” (Tatarskii 1971), which give the overall wavefront structure function, $D(r)$, as the sum of the wavefront structure functions of individual turbulent layers as

$$D(r) = \sum_i D_i(r), \quad (9)$$

where $D_i(r)$ is the structure function of the i^{th} layer. It is also assumed that the wavefront error is mostly in phase, not in amplitude or scintillation, which should be valid at a representative astronomical site like Mauna Kea. Therefore $D(r)$ can be regarded as a phase structure function and

$$D_i(r) = 2.91 \left(\frac{2\pi}{\lambda_{SCI}} \right)^2 \cdot \int_i C_n^2(h) dh \cdot r^{5/3}, \quad (10)$$

where $\int_i dh$ indicates the integral over the i^{th} turbulent layer. We adopt the six-layer turbulence model employed by Guyon (2005) to approximate the conditions above Mauna Kea (Table 4 of Guyon 2005). The i^{th} turbulent layer is characterized by the altitude, h_i , and the fractional contribution to the integrated $C_n^2(h)$, F_i , or,

$$F_i = \frac{\int_i C_n^2(h)dh}{\int_{H_T}^{H_{MAX}} C_n^2(h)dh}, \quad (11)$$

where the physical thickness of the i^{th} layer is negligible compared to the entire thickness of the atmosphere.

The wavefront variance associated with this layer is,

$$\begin{aligned} \sigma_i^2 &= D_i(r(\lambda_{WFS}, \lambda_{SCI}, h_i)) \\ &= 2.91 \left(\frac{2\pi}{\lambda_{SCI}} \right)^2 F_i \cdot \int_{H_T}^{H_{MAX}} C_n^2(h)dh \cdot r(\lambda_{WFS}, \lambda_{SCI}, h_i)^{5/3} / \cos z_0, \end{aligned} \quad (12)$$

Note that the factor $1/\cos z_0$ is necessary, since the integrated C_n^2 is given for the propagation toward the zenith, while the actual light path through the layer of isotropic turbulence is longer by this factor. Here the small variance caused by the difference in the optical path lengths at the two wavelengths is neglected. We obtain the total variance $\sigma^2(\lambda_{WFS}, \lambda_{SCI}, z_0)$ by

$$\sigma^2(\lambda_{WFS}, \lambda_{SCI}, z_0) = \sum_{i=1}^6 \sigma_i^2. \quad (13)$$

Computer programming is carried out in C, and source codes are available upon request to the author. As long as the multi-layer turbulence model is adopted, they can be modified easily for other astronomical sites.

3. Results

Typical situations are that λ_{WFS} is in the visible and λ_{SCI} is in the near-infrared. In addition, we also explore the possibility of using an infrared wavefront sensor.

For a typical CCD detector, the quantum efficiency (QE) peaks around $0.7 \mu\text{m}$, while a full-depletion type CCD with high QE at longer wavelengths may be used at around $0.9 \mu\text{m}$ (Groom et al. 2000; Strüder et al. 2000; Kamata et al. 2004). The infrared wavefront sensor must be operated through atmospheric windows, namely at J ($1.25 \mu\text{m}$), H ($1.65 \mu\text{m}$), or K ($2.2 \mu\text{m}$). One potential disadvantage in the infrared is that sky background is much higher than in the visible, especially at H due to OH airglow and at K due to both OH airglow and thermal emission. Although we include the case for wavefront sensing at H and science imaging at K , a realistic long wavelength limit may be $1.25 \mu\text{m}$, where sky background is still tolerable. To summarize, we consider the cases for $\lambda_{WFS} = 0.7, 0.9, 1.25,$ and $1.65 \mu\text{m}$, and $\lambda_{SCI} = 1.25, 1.65,$ and $2.2 \mu\text{m}$.

For the seeing condition, we choose a typical value for Mauna Kea, $r_0 = 0.2$ m at $0.5\mu\text{m}$, which corresponds to a half arcsecond seeing in the visible. Since the wavefront variance scales as $(0.2/r_0)^{5/3}$, it is sufficient to present the results only for a single value of r_0 . However, when we need to estimate the variance for a site other than Mauna Kea, this scaling does not necessarily hold, since the altitudes and strengths of individual turbulent layers determine the overall wavefront variance.

Results are plotted as the zenith angle vs. $\log_{10} \sigma^2$, for $\lambda_{SCI} = 1.25, 1.65$, and $2.2 \mu\text{m}$ respectively in Figs 1, 2, and 3. For another seeing condition characterized by r_0 , variances are obtained by shifting individual curves by $(5/3) \log_{10}(0.2/r_0)$. Since the Strehl ratio, S , is given by

$$S = \exp(-\sigma^2), \quad (14)$$

or for a small σ^2 ,

$$S \approx 1 - \sigma^2, \quad (15)$$

(Tyson, R. K. 1991).

Therefore, $\log_{10} \sigma^2 = -2$ and -1 , correspond to $S = 0.99$ and 0.90 respectively.

Another way of presenting our results is to show the behavior of the maximum allowed zenith distance as a function of λ_{WFS} , for a given set of λ_{SCI} and the tolerance level of the wavefront variance. In Figs 4, 5 and 6, such plots are given for $\lambda_{SCI} = 1.25, 1.65$, and $2.2 \mu\text{m}$, for the cases of $\sigma^2 = 0.01$ and 0.05 .

4. Discussion

4.1. Significance of High Altitude Turbulence

To see the relative contribution of each layer, its altitude relative to the summit of Mauna Kea (4.2 km), the beam separation r_i in cm, the phase variance, σ_i^2 in rad^2 are given for $\lambda_{SCI} = 1.65 \mu\text{m}$, $\lambda_{WFS} = 0.7 \mu\text{m}$, and $z = 50^\circ$ in Table 1. The total wavefront variance for this case is about 0.01. Two factors that determine the relative significance of each layer, are the fractional integrated C_n^2 , F_i , and beam separation r_i , since $\sigma_i^2 \propto F_i \cdot r_i^{5/3}$. The largest contribution comes from the layer 8 km above the Mauna Kea Observatory. r_i at a high altitude is order of a few cm.

4.2. Is the Chromatic Shear a Limiting Factor for the Next Generation Extreme AO System?

If we consider a Shack-Hartman sensor with a 512×512 pixel CCD, attached to an 8 m telescope, the wavefront sampling interval is 1.6 cm, comparable to r_i . On the other hand, an ExAO currently designed will have about 2000 actuators, or 50 actuators across the diameter of the telescope aperture, corresponding to 16 cm sampling interval. The residual wavefront variance, σ_{AO}^2 associated with the finite actuator spacing will be given by

$$\sigma_{AO}^2 = 0.1C \left(\frac{0.16}{r_0} \right)^{5/3}, \quad (16)$$

where the constant C depends on the actual 2D configuration of the actuator, and is order of unity, assuming that the tip/tilt component of the wavefront error is removed on the spatial scale of the actuator interval. Even if some other low-order Zernike terms are corrected, there will not be a major change in C , since the major part of the wavefront variance is due to the tip/tilt effect (Noll 1976). For instance, $C = 1.34$ for a 16-cm-diameter tip/tilt-corrected circular aperture (Noll 1976). For a finite zenith distance,

$$\sigma_{AO}^2(z) = 0.1C \left(\frac{0.16}{r_0(\lambda_{SCI})} \right)^{5/3} / \cos z, \quad (17)$$

since the path length through the turbulent atmosphere is longer by $1/\cos z$. When the seeing condition is characterized by $r_0 = 0.2 \mu\text{m}$, at $\lambda = 0.5 \mu\text{m}$,

$$r_0(\lambda_{SCI}) = 0.2 \cdot \left(\frac{\lambda_{SCI}}{0.5} \right)^{1.2}. \quad (18)$$

$$\sigma_{AO}^2(z) = 0.0172C \frac{1}{\lambda_{SCI}^2 \cdot \cos z}, \quad (19)$$

At $z = 50^\circ$, $\sigma_{AO}^2 = 0.017C, 0.0098C$, and $0.0055C$ respectively at $\lambda_{SCI} = 1.25, 1.65$ and $2.2 \mu\text{m}$. Remember that $\sigma^2 = 0.01$ was obtained for $\lambda_{SCI} = 1.65 \mu\text{m}$, $\lambda_{WFS} = 0.7 \mu\text{m}$, $z = 50^\circ$ for the pure CS effect given in Table 1. Therefore at this zenith distance, wavefront errors originating from the finite actuator spacing (FAS) and the CS effect appear comparable. However z -dependencies of two effects are different. The variance due to the CS effect approximately depends on z as $(\sin z)^{5/3} \cdot (1/\cos z)^{13/3}$, while that due to the FAS effect goes as $1/\cos z$. Therefore the former is a much faster increasing function of z . At $z < 50^\circ$, the FAS effect is dominant, while at $z > 50^\circ$, the CS effect becomes dominant. This parameter combination is of practical interest, since $\lambda_{WFS} = 0.7 \mu\text{m}$ represents the operational wavelength of a commonly used wavefront sensor and $\lambda_{SCI} = 1.65$

μm is considered to be the prime wavelength band for simultaneous differential imaging aiming at detecting giant planets having methane bands using a room-temperature coronagraph.

4.3. Spatial Frequency Dependence of the Chromatic Shear

In the previous subsection, we compared only the total wavefront variances due to the CS and FAS effects. However, the spatial power spectra of the two effects are expected to be different and here we discuss this difference qualitatively.

The CS effect preserves the original Kolmogorov spectrum, including low frequency components. Therefore at the focal plane, it degrades the target star PSF at small angular radii. So the detectability of a close-in planet is reduced by the CS effect.

On the other hand, the AO correction works as a high-pass filter of the Kolmogorov spectrum, and the residual power spectrum due to the FAS effect has finite values mainly at high frequencies. At the focal plane, the PSF envelope at a radius, $2''$ or greater is affected for the 8 m telescope at $\lambda_{SCI} = 1.65 \mu\text{m}$. High frequency phase fluctuations produce extended scattered light at the focal plane, which is in competition with OH sky background of 13.4 mag per \square'' (Cox 1999).

4.4. More on the Next Generation Extreme AO System

From the previous subsection, we have seen that there will be a transition zenith distance, z_{TR} , at which the wavefront variance due to the FAS effect dominating the wavefront error at $z < z_{TR}$ and that due to the CS effect dominating the wavefront error at $z > z_{TR}$, cross over. Here we wish to shift z_{TR} as large as possible. The quantitative optimization process depends on the actual design of an ExAO system, whose consideration is beyond the scope of this paper. Here we only list up some issues to be considered.

A simple-minded solution is to shift λ_{WFS} to a longer wavelength. However many practical issues arise in reality.

The first issue is sky background, which we have already mentioned before. Actually a smaller λ_{WFS} is preferred, if this effect is dominant. Only planets with large angular separations from their main stars are affected by sky background. Depending on the Strehl ratio of the system, the FAS effect, which is larger for a smaller λ_{WFS} , may dominate the background instead of the sky background as mentioned above.

The second issue is related to the detector performance, whose situation may change in the near future. It is not the quantum efficiency, which is already high enough both in the visible and near infrared, but the read-noise level, which can be a significant issue, due to the fast temporal sampling of the wavefront and a small collecting area per actuator. A currently available infrared

array typically has a read-noise level of about $10 e^-$ per pixel, and may even be higher for a higher sampling rate. Actually at this read noise level, it is not sky background, but the read noise that determines the signal-to-noise ratio. Unless a low-noise infrared detector happens to become available, it may be realistic to choose a visible detector.

One may try to optimize the performance of the wavefront sensor by the combination of a red-sensitive CCD and a long-pass filter to reject blue photons, which behave as a noise source when the CS effect is dominant, provided that the red-sensitive CCD shows a low read-noise level even for a high sampling rate. However the quantitative analysis should take into account many factors including the spectral energy distribution of a target star, and further general discussion may not be of a major practical use.

We might have underestimated the instrumental error associated with a non-ideal adaptive optics system. So the actual instrumental error may be larger than that estimated from the FAS effect alone. If this is the case, a true z_{TR} will be larger than that estimated above.

5. Concluding Remark

We have obtained the wavefront variance due to atmospheric non-common path error, or chromatic shear, as a function of wavelengths for wavefront sensing and science imaging, and zenith distance, assuming an idealized adaptive optics system with a very fine actuator interval for wavefront correction. For visible wavefront sensing and infrared science imaging, the wavefront variance exceeds 0.01 at $z \sim 50^\circ$. For an extreme AO system currently designed, the residual error due to the finite actuator spacing, appears to dominate the wavefront error at $z < 50^\circ$ and the non-common path effect may become dominant only at $z > 50^\circ$.

The author thanks Olivier Guyon and the referee, Eugene Pluzhnik, for helpful comments on the manuscript of this paper.

REFERENCES

- Cox, A. N. 1999, Ed. *Allen's Astrophysical Quantities*, Fourth Edition, AIP Press, Springer, NY
- Fried, D. L. 1966, *J. Opt. Soc. Am.*, 56, 1372
- Groom, D. E. et al. 2000, *Nucl. Instr. and Meth. A* 442, 216
- Guyon, O. 2005, *ApJ*, 629, 592
- Kamata, Y. et al. 2004, *Proc. SPIE*, 5499, 210
- Noll, R. J. 1976, *J. Opt. Soc. Am.*, 66, 207

Strüder, L. et al. 2000, Proc. SPIE, 4012, 200

Tatarskii, V. I. 1971. *The Effects of the Turbulent Atmosphere on Wave Propagation*, translated from Russian by Israel Program for Scientific Translations

Tyson, R. K. 1991. *Principle of Adaptive Optics*, Boston Academic Press

Layer	Altitude km (above Mauna Kea)	Fractional $\int C_n^2 dh$	Beam Separation cm	Wavefront Variance rad ²
1	0.5	0.2283	0.17	7.98×10^{-5}
2	1.0	0.0883	0.30	8.14×10^{-5}
3	2.0	0.0666	0.57	1.78×10^{-4}
4	4.0	0.1458	1.04	1.04×10^{-3}
5	8.0	0.3350	1.68	5.34×10^{-3}
6	16.0	0.1350	2.22	3.42×10^{-3}
Total		1.0		1.01×10^{-2}

Table 1: Relative Contribution of Each Turbulent Layer. $\lambda_{SCI} = 1.65 \mu\text{m}$, $\lambda_{WFS} = 0.7 \mu\text{m}$ and $z = 50^\circ$. This six-layer model is adopted from Guyon (2005).

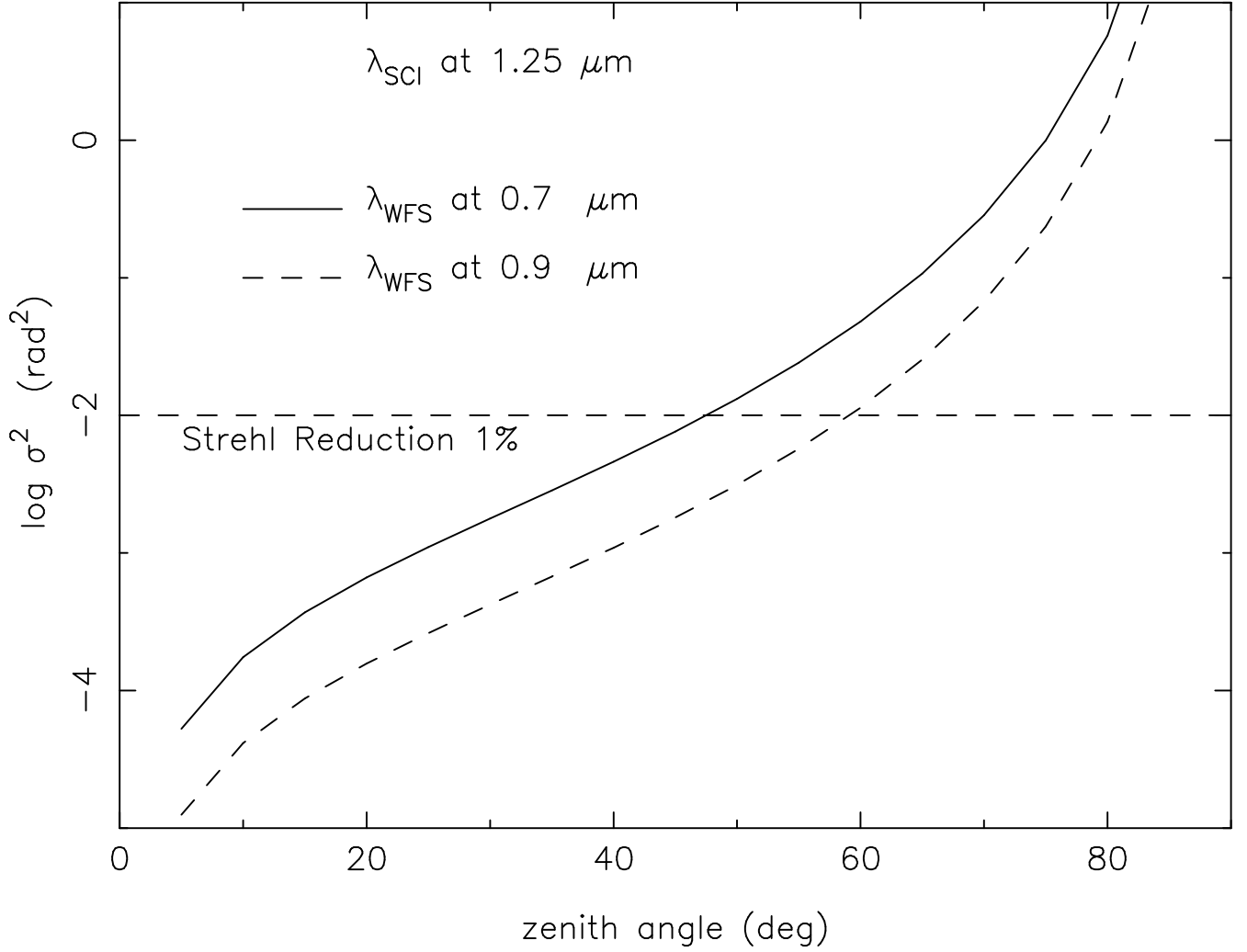


Fig. 1.— Wavefront variance due to atmospheric non-common path effect. $\lambda_{SCI} = 1.25 \mu\text{m}$. Assumed seeing condition is $r_0 = 0.2\text{m}$ at $\lambda = 0.5 \mu\text{m}$. The variance for an arbitrary r_0 can be obtained by shifting each curve vertically by $(5/3) \log_{10}(0.2/r_0)$.

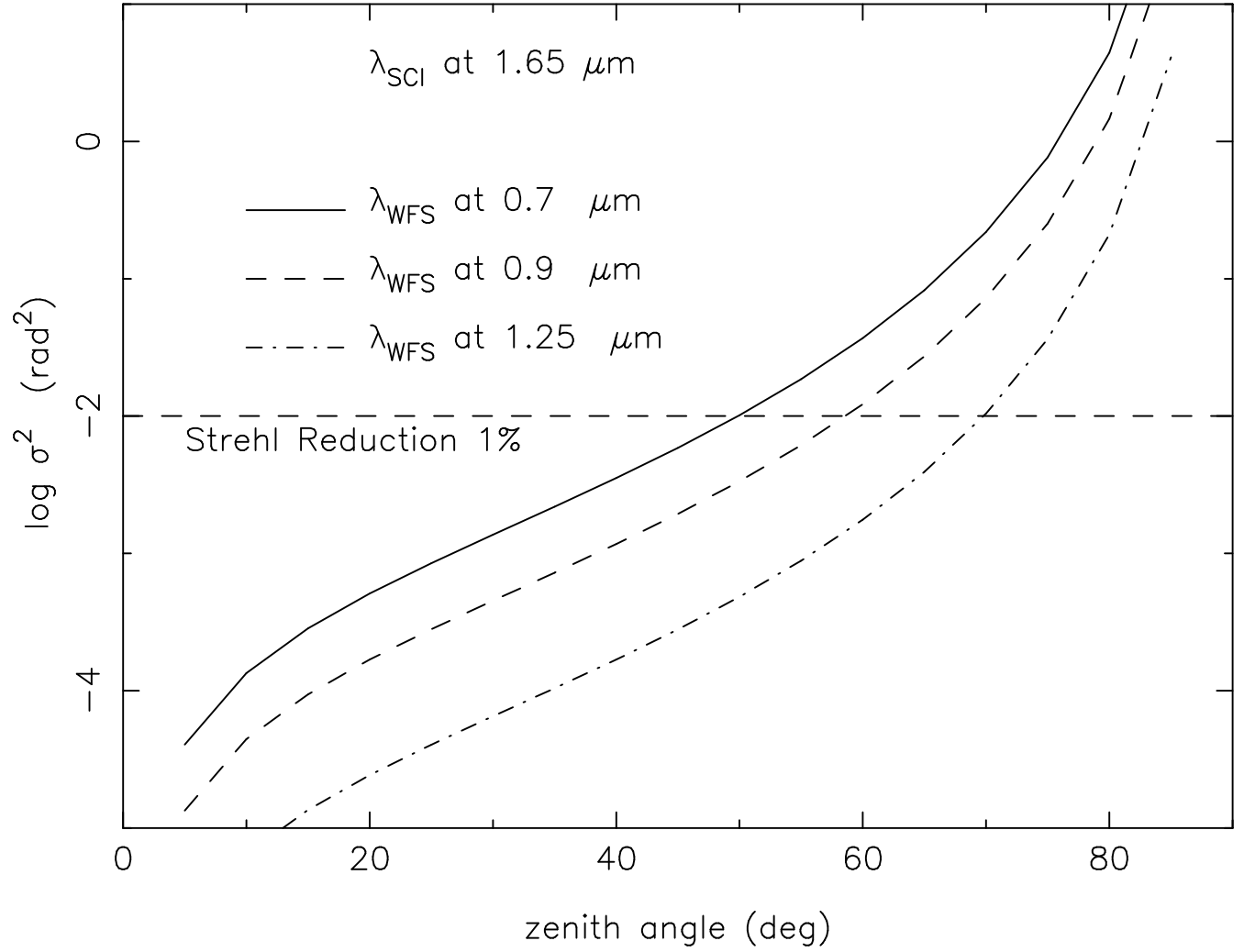


Fig. 2.— Wavefront variance due to atmospheric non-common path effect. $\lambda_{SCI} = 1.65 \mu\text{m}$.

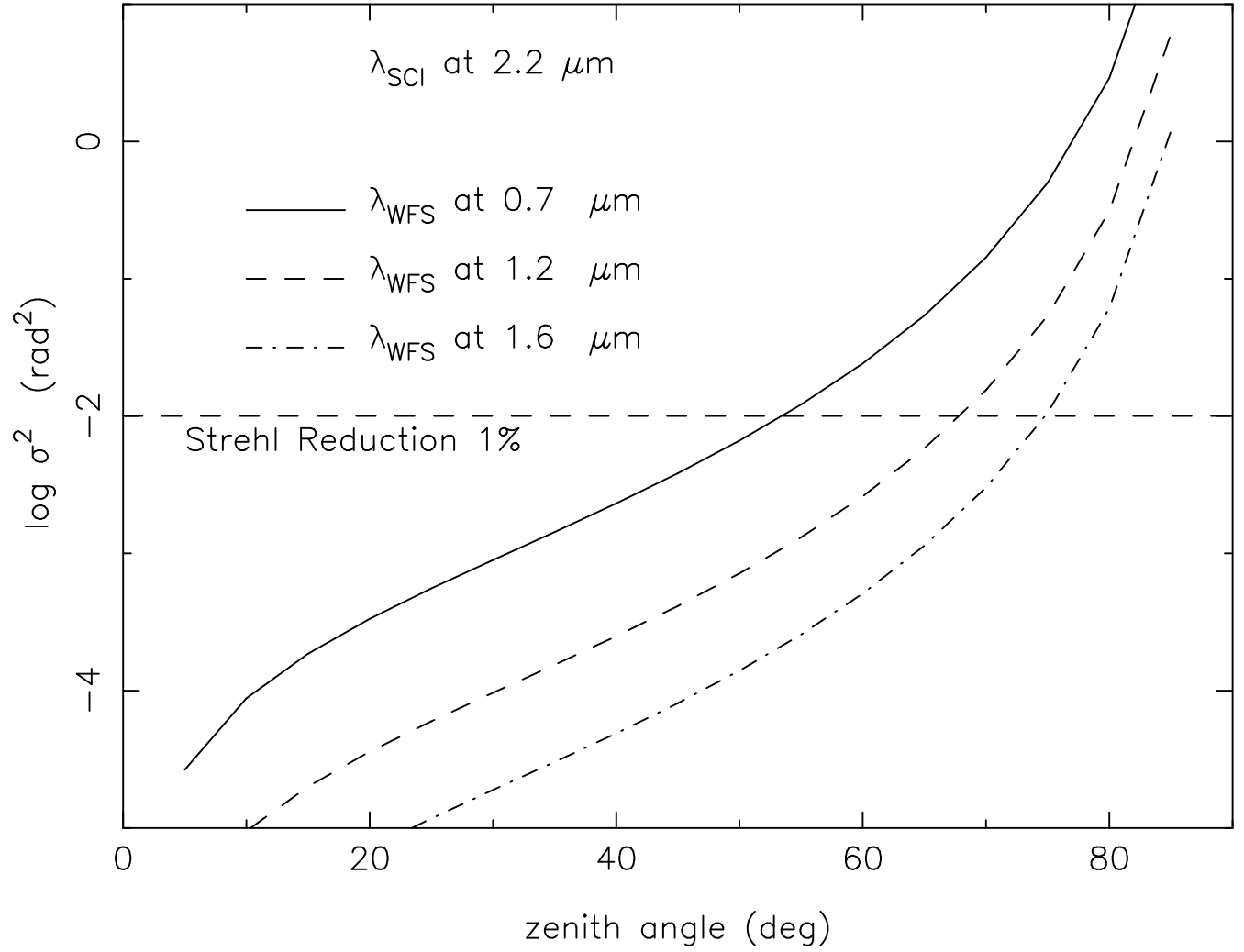


Fig. 3.— Wavefront variance due to atmospheric non-common path effect. $\lambda_{SCI} = 2.2 \mu\text{m}$.

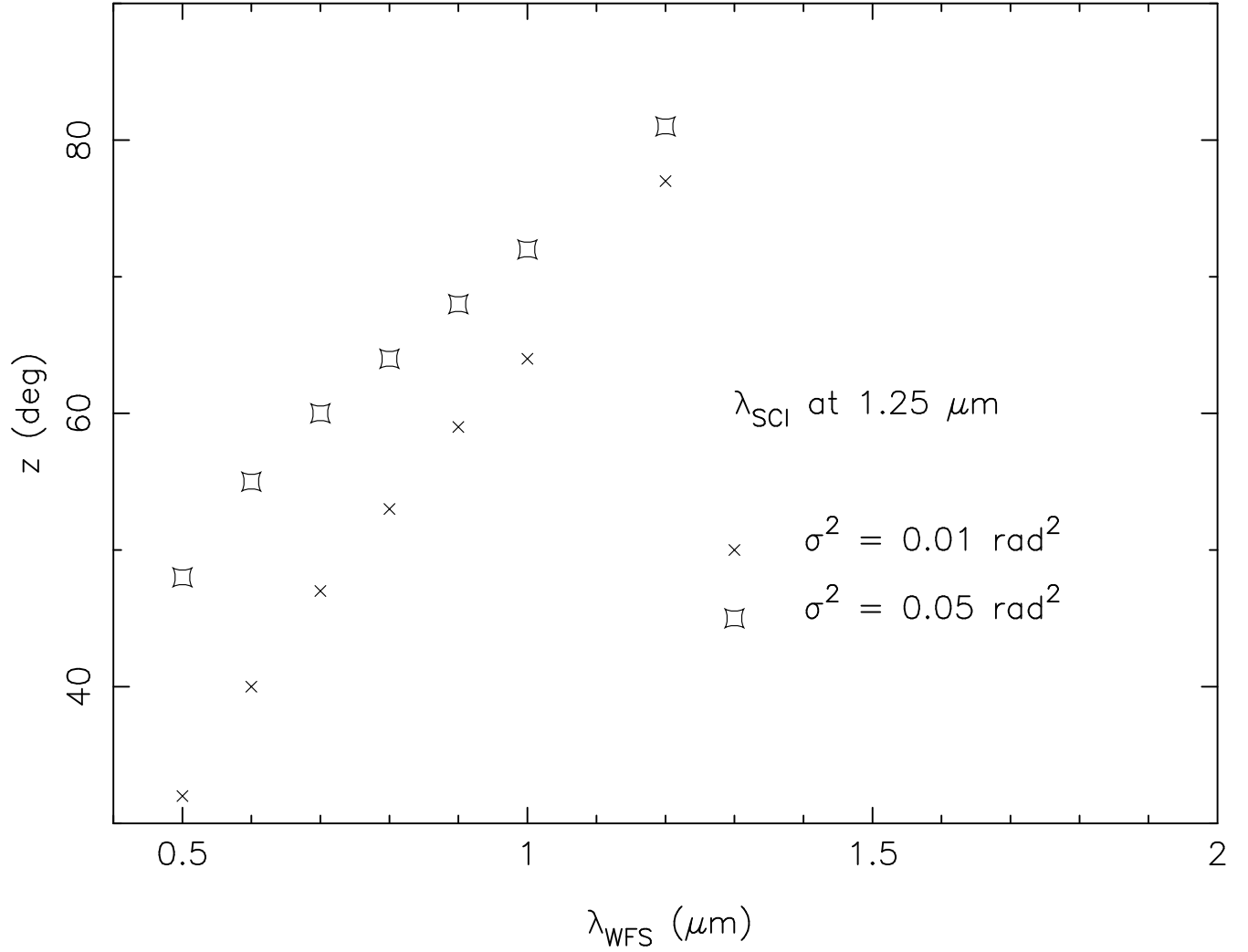


Fig. 4.— Wavelength dependencies of zenith distances giving $\sigma^2 = 0.01$ and 0.05 . $\lambda_{\text{SCI}} = 1.25 \mu\text{m}$.

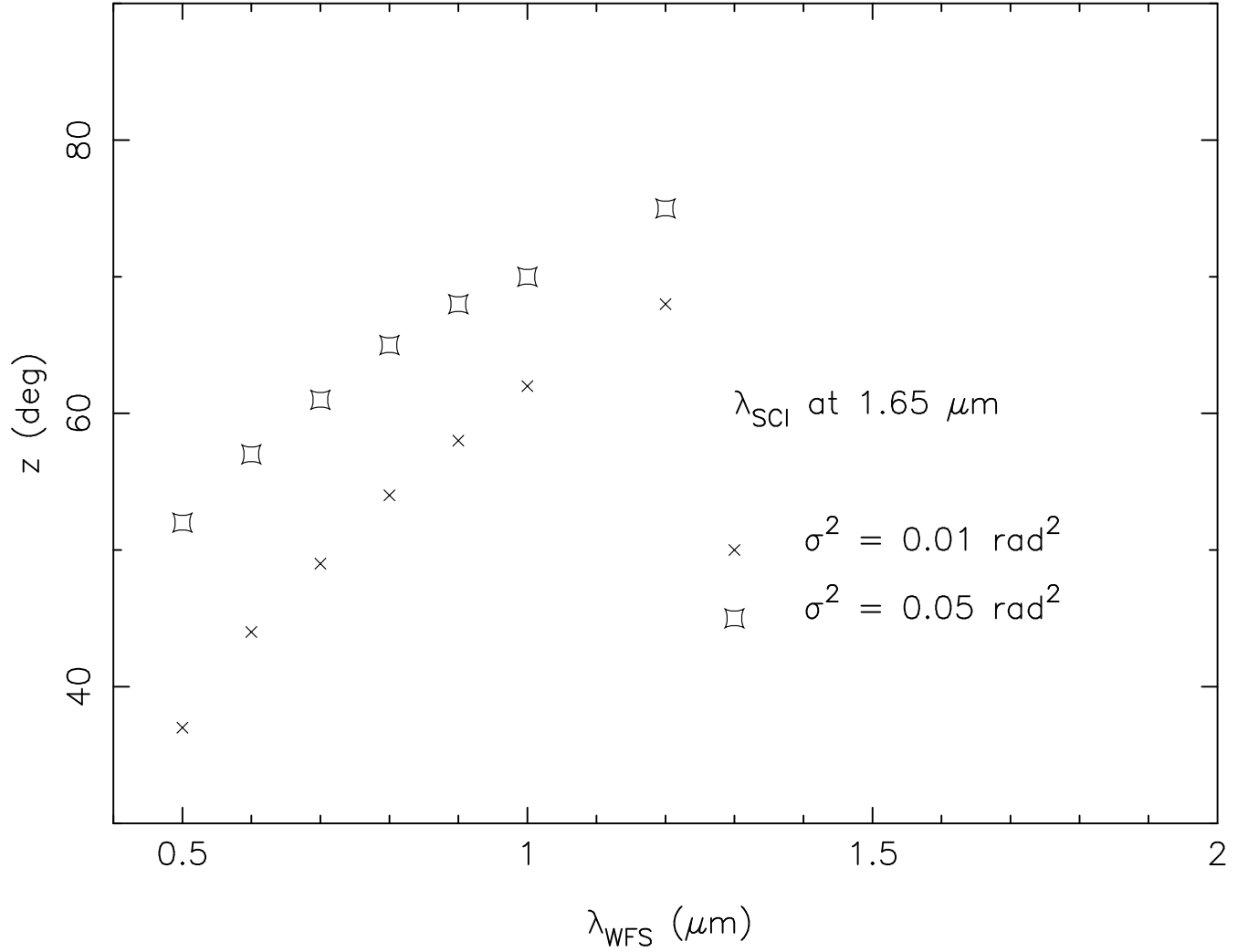


Fig. 5.— Wavelength dependencies of zenith distances giving $\sigma^2 = 0.01$ and 0.05 . $\lambda_{\text{SCI}} = 1.65 \mu\text{m}$.

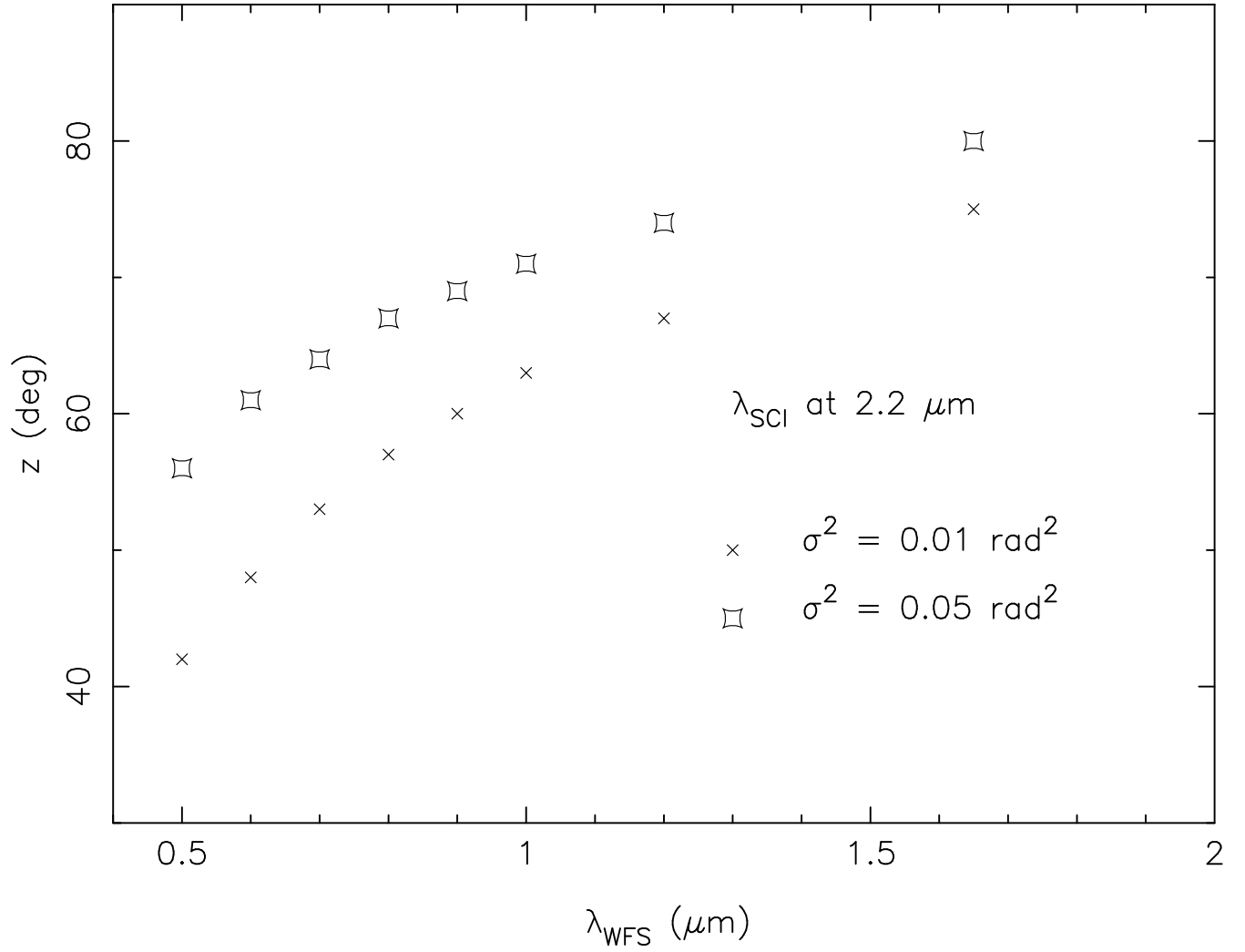


Fig. 6.— Wavelength dependencies of zenith distances giving $\sigma^2 = 0.01$ and 0.05 . $\lambda_{\text{SCI}} = 2.2 \mu\text{m}$.